RSC Advances

PAPER

View Article Online
View Journal | View Issue

Check for updates

Cite this: *RSC Adv.*, 2026, **16**, 3220

Preparation of chitosan-EDTA bifunctionally modified magnetic walnut shell biochar and study on its copper ion (Cu(II)) adsorption performance

Xuejian Zhou, [a] Yufei Yang,[a] Ruiqi Yang,[a] Lei Shi,[a] Ling Zhou*[a] and Xifeng Lv*[ab]

This study aims to address the limitations of existing adsorbents in treating copper(II)-containing wastewater by developing a high-performance and highly practical adsorbent. A chitosan-EDTA bifunctional modified magnetic walnut shell biochar (E-CMBC) was synthesized *via* a three-step method: magnetic modification of walnut shell biochar with Fe_3O_4 nanoparticles, surface coating with chitosan, and grafting of EDTA *via* amide bond coupling. The physicochemical properties of E-CMBC were characterized using field emission scanning electron microscopy (FE-SEM), Fourier transform infrared spectroscopy (FTIR), X-ray diffraction (XRD), Brunauer–Emmett–Teller (BET) analysis, Thermogravimetric (TGA) analysis and zeta potential measurement, and its adsorption performance for copper(II) was systematically evaluated through batch experiments. Key results demonstrate that the maximum adsorption capacity of E-CMBC for copper(II) reaches 130.8 mg g^{-1}, with 52.4% of the equilibrium capacity achieved within 15 min; the adsorption process conforms to the pseudo-second-order kinetic model and the Langmuir isotherm model, confirming that chemical chelation is the dominant mechanism, and thermodynamic analysis indicates that the adsorption process is spontaneous and endothermic, with entropy increase serving as the primary driving force. Notably, E-CMBC maintains high adsorption efficiency within the pH range of 3–5, exhibits strong selectivity against coexisting ions (Na^+, K^+, Ca^{2+}, Mg^{2+}), enables rapid magnetic separation within seconds, and retains 91.13% of its initial adsorption capacity after five adsorption–desorption cycles. By integrating the combined advantages of EDTA (high selectivity), chitosan (abundant complexation sites), and magnetic biochar (easy separation), this study fills the gaps in existing literature and provides an efficient, sustainable, and engineering-applicable solution for heavy metal pollution control and high-value utilization of agricultural waste.

Received 15th November 2025
Accepted 4th January 2026

DOI: 10.1039/d5ra08820h

rsc.li/rsc-advances

Open Access Article. Published on 14 January 2026. Downloaded on 4/6/2026 1:23:54 AM.
This article is licensed under a Creative Commons Attribution-NonCommercial 3.0 Unported Licence.

1 Introduction

Accelerated industrialization has made heavy metal pollution a severe global environmental challenge.[1–3] Copper ions (Cu(II)) enter wastewater through various sources including electroplating, metal refining, mining,[4] paint/printing processes,[5] pharmaceuticals/pesticides production,[6] and electronics manufacturing, posing significant environmental risks.[7] Notably, Cu(II) has emerged as a prominent contaminant in groundwater resources,[8] further expanding its scope of harm. Although copper is an essential trace element, its excessive accumulation induces severe toxic effects: it disrupts aquatic microbial communities and ecological balance, and poses grave threats to human health—beyond damaging the liver and kidneys,[9,10] excessive intake can lead to brain injury as well as a range of diseases such as Wilson's disease, Parkinson's disease, Alzheimer's disease, prion diseases, and Meniere's disease.[11,12] Current mainstream technologies—including chemical precipitation,[13] ion exchange,[14,15] and membrane separation[16]—have significant limitations in terms of treatment efficiency, secondary pollution control, operating costs, and applicability to low-concentration wastewater. In contrast, adsorption is considered the most promising method for industrial application because it is simple to operate, relatively low-cost, and effective in removing low-concentration pollutants. However, the key challenge lies in developing new adsorbents that have high adsorption capacity, good selectivity, strong stability, and practical engineering value—especially easy separation and recovery.[14]

At present, various adsorbents (*e.g.*, activated carbon,[17] porous carbon nanofibers,[18] graphene, and cation exchange resins[19]) have been used to remove Cu(II) from aqueous solutions. However, these materials generally have problems such as single functionality, limited specific surface area, insufficient selectivity, or high cost, which restrict their adsorption efficiency and practical application potential. To overcome this

[a]*College of Chemistry and Chemical Engineering, Engineering Laboratory of Chemical Resources Utilization in South Xinjiang of Xinjiang Production and Construction Corps, Tarim University, Alar 843300, China. E-mail: lvning7431@163.com*
[b]*Modern Agricultural Engineering Key Laboratory at Universities of Education, Department of Xinjiang Uygur Autonomous Region, Alar, Xinjiang 843300, China*

© 2026 The Author(s). Published by the Royal Society of Chemistry

Open Access Article. Published on 14 January 2026. Downloaded on 4/6/2026 1:23:54 AM. This article is licensed under a Creative Commons Attribution-NonCommercial 3.0 Unported Licence.

bottleneck, a surface functional modification strategy has been proposed: by introducing specific functional groups with high affinity and selectivity for target pollutants, targeted recognition and efficient removal of target pollutants can be achieved.[20] Biochar is a carbon-rich material produced by the pyrolysis of biomass under oxygen-limited conditions. It has advantages such as wide raw material sources (especially agricultural wastes), low cost, environmental friendliness, large specific surface area, abundant pores, and rich oxygen-containing functional groups (*e.g.*, carboxyl groups, hydroxyl groups) on its surface—making it a highly promising adsorption matrix.[21] Among various biomass sources, walnut shells are abundant agricultural and forestry wastes; the biochar derived from them has unique pore structures and surface chemical properties, making it a valuable precursor for adsorbents.

However, conventional biochar powders face engineering challenges in wastewater treatment, such as difficult solid–liquid separation and inconvenient recovery/reuse. Magnetic modification (by adding components like Fe_3O_4 to the biochar matrix) can give biochar superparamagnetism, enabling rapid and efficient solid–liquid separation under an external magnetic field greatly improving the practical value of the adsorbent.[22] Furthermore, surface chemical modification is necessary to further enhance the adsorption capacity and selectivity for Cu(II). Chitosan (CS) is a natural cationic polysaccharide containing abundant free amino ($-NH_2$) and hydroxyl (–OH) groups. These functional groups have strong binding affinity for heavy metal ions like Cu(II), making chitosan a common surface modifier for biochar.[23] Emamy *et al.*[24] developed a nitrogen-enriched chitosan activated carbon (nitrogen content of about 16 wt%, specific surface area of 1556 $m^2\ g^{-1}$), which removed more than 99% of Cr(VI) at pH = 2, and Pb(II) at pH = 4–6, suggesting that it is highly efficient for heavy metal remediation. Peralta *et al.*[25] developed a magnetic chitosan composite (MCC) that effectively removed Pb(II) (220.9 mg g^{-1}), Cu(II) (216.8 mg g^{-1}), and Ni(II) (108.9 mg g^{-1}) from water within 120 minutes, and could be magnetically recovered. Ethylenediaminetetraacetic acid (EDTA) is a classic multidentate chelating agent with multiple coordination atoms (nitrogen and oxygen). It forms highly stable water-soluble complexes with metal ions like Cu(II), showing excellent selectivity and high binding constants.[26] Wang *et al.*[27] developed an efficient heavy metal adsorbent (EDTA@BP/PP) by grafting EDTA onto banana/pomegranate peels. This material showed significantly enhanced adsorption capacities for Cd(II), Co(II), Mn(II), and Ni(II) (up to 86.96 mg g^{-1}), achieving equilibrium within 5 minutes. The mechanism involves synergistic ion exchange and surface complexation.

This study proposes a new type of chitosan-EDTA bifunctionally modified magnetic walnut shell biochar (E-CMBC). Its design leverages the complementary advantages of individual components: walnut shell biochar acts as an eco-friendly, low-cost substrate with a large specific surface area and porosity; Fe_3O_4 nanoparticles enable rapid magnetic separation; chitosan provides abundant functional groups ($-NH_2$/–OH) to enhance Cu(II) complexation; and EDTA acts as a strong chelating ligand to improve selectivity and binding affinity for Cu(II). This bifunctional modification strategy is expected to reduce the stability limitations of individual components in acidic environments, while significantly improving Cu(II) adsorption efficiency through the combined effects of distinct functional groups. This study systematically explores the synthesis of E-CMBC, characterizes its physicochemical properties, evaluates its Cu(II) adsorption performance in aqueous solutions, and clarifies the underlying adsorption mechanism. It provides a theoretical basis and technical support for developing efficient, renewable, and engineering-applicable adsorbents for heavy metal removal.

2 Materials and methods

2.1 Materials

All chemicals used were of analytical grade (AR), sourced as follows: ethylenediaminetetraacetic acid (EDTA) was purchased from Tianjin Zhiyuan Chemical Reagent Co., Ltd (Tianjin, China); sodium hydroxide (NaOH), hydrochloric acid (HCl), and copper(II) sulfate pentahydrate ($CuSO4\cdot5H_2O$) were obtained from Tianjin Beichen Fangzheng Reagent Factory (Tianjin, China); chitosan (degree of deacetylation ≥95%) and glacial acetic acid were bought from Tianjin Bohua Chemical Reagent Co., Ltd (Tianjin, China); 1-ethyl-3-(3-dimethylaminopropyl) carbodiimide hydrochloride (EDC HCl) was sourced from Tianjin Zhiyuan Chemical Reagent Co., Ltd (Tianjin, China). Walnut shells were collected from Aksu, Xinjiang Uygur Autonomous Region, China.

2.2 Adsorbent synthesis

2.2.1 Synthesis of magnetic walnut shell biochar (MBC). 20 g of walnut shell powder was soaked in 200 mL of 1 mol L^{-1} $FeSO_4\cdot7H_2O$ solution and shaken for 12 h. After filtration, the residue was dried at 85 °C for 12 h. The dried sample was pyrolyzed in a tube furnace under N_2 flow (200 mL min^{-1}) at a heating rate of 5 °C min^{-1} to 700 °C (held for 2 h). After cooling naturally to room temperature, the product was repeatedly washed with deionized water until the pH became neutral (~7). It was then vacuum-dried at 60 °C for 12 hours, ground, and sieved through a 200-mesh sieve to obtain MBC.

2.2.2 Chitosan-modified MBC (CMBC). Dissolve 1.5 g of chitosan in 150 mL of 2% (v/v) acetic acid solution and stir continuously until the chitosan is completely dissolved. Then add 1.5 g of MBC and continue to stir for 2 hours to ensure that MBC is fully mixed with the chitosan solution. The pH value of the above mixture was adjusted to 10.0 ± 0.2 with 1% (w/v) NaOH solution, and then the static cross-linking reaction was carried out at room temperature for 12 hours. After the cross-linking was completed, the solid product was collected by filtration, washed with deionized water until the filtrate was neutral pH, and then dried at 65 °C for 12 hours. After drying, it was sieved through a 200-mesh screen to obtain chitosan-modified biochar (CMBC).

2.2.3 EDTA-chitosan bifunctionalized MBC (E-CMBC). 3 g of CMBC and 3 g of EDTA were dispersed in 300 mL of deionized water and pre-activated at 60 °C for 4 hours to fully expose the

Open Access Article. Published on 14 January 2026. Downloaded on 4/6/2026 1:23:54 AM. This article is licensed under a Creative Commons Attribution-NonCommercial 3.0 Unported Licence.

carboxyl groups (–COOH) of chitosan molecules on the surface of CMBC and the amino groups ($-NH_2$) of EDTA molecules. After cooling to 40 °C, add 15 mL of 1 mol L^{-1} sodium hydroxide and 2.8 g of EDC HCl in sequence. The mixture was stirred at 40 °C for 2 hours and then stirred at room temperature for 12 hours to promote the formation of a stable amide bond (–CONH–) with the $-NH_2$ of EDTA, ensuring that EDTA was firmly bound to the surface of CMBC and preventing the modifier from falling off during the subsequent adsorption process. Filter the product and alternately wash it with 0.1 mol L^{-1} sodium hydroxide, deionized water, 0.1 mol L^{-1} hydrochloric acid and deionized water until the pH is neutral. After vacuum drying at 60 °C for 12 hours, the material was passed through a 200-mesh sieve to obtain E-CMBC.

2.3 Characterization

The concentration of Cu(II) was measured using a ContrAA 300 flame atomic absorption spectrometer (FAAS, Analytik Jena AG, Jena, Germany) at 324.8 nm with standard calibration. Morphological characteristics were analyzed using a field-emission scanning electron microscope (FE-SEM, JSM-7800F, JEOL Ltd, Tokyo, Japan) with energy-dispersive spectroscopy (EDS) at an accelerating voltage of 5 kV. The surface area and pore structure were determined *via* nitrogen physisorption at 77 K using an Autosorb-iQ 4000e analyzer (Quantachrome Instruments, Boynton Beach, FL, USA). The BET surface area and BJH pore size distribution were calculated after 6 hours of vacuum degassing at 150 °C. Surface functional groups were identified using a Fourier-transform infrared spectrometer (FT-IR, IRTracer-100, Shimadzu Corp., Kyoto, Japan) with KBr pellets (scanning range: 400–4000 cm^{-1}, resolution: 4 cm^{-1}, 32 scans). Crystalline structure was characterized using an X-ray diffractometer (XRD, D8 Advance, Bruker AXS, Karlsruhe, Germany) with Cu-Kα radiation ($\lambda = 1.5406$ Å, scanning range: 5–80° 2θ, step size: 0.02°, scan rate: 2° min^{-1}). Thermogravimetric (TGA) analysis was performed using a synchronous thermal analyzer (STA 449 F5, Netzsch GmbH, Selb, Germany) to quantify the grafting amount of modifiers and evaluate thermal stability. Prior to testing, all samples were vacuum-dried at 60 °C for 12 hours to remove adsorbed water. The tests were conducted under a high-purity nitrogen atmosphere (flow rate: 20 mL min^{-1}) with a temperature range of 30–800 °C and a heating rate of 10°C min^{-1}. Surface charge was evaluated *via* zeta potential analysis (Zetasizer Nano ZS90, Malvern Panalytical, Malvern, UK) over a pH range of 1–5.

2.4 Adsorption experiments

A 1000 mg L^{-1} Cu(II) stock solution was prepared by dissolving 3.93 g of $CuSO_4 \cdot 5H_2O$ in ultrapure water, and working solutions were prepared by diluting this stock. Batch adsorption experiments were conducted in temperature-controlled shakers to evaluate factors affecting Cu(II) removal. All experiments were set with three parallel repetitions. The final results were expressed as the average of three parallel experiments. The experiments had good repeatability, ensuring the reliability of the data. 100 mL of Cu(II) solution (30–120 mg L^{-1}) and a certain amount of adsorbent (0.02–0.1 g) were added to 250 mL conical flasks. The effect of pH was studied by adjusting the initial pH to 1.0–5.0 with dilute NaOH/HCl. The effect of temperature was examined at a fixed pH of 3.0 within 25–45 °C. The effect of adsorbent dosage was tested by varying the adsorbent mass (0.02–0.1 g) under fixed Cu(II) concentration, pH, and temperature. Adsorption kinetics were monitored at time intervals (0–180 min) until equilibrium. Adsorption isotherms were obtained at 45 °C (0.04 g adsorbent, pH 3.0) with initial Cu(II) concentrations of 30–120 mg L^{-1}. Adsorption thermodynamics were studied at 25–45 °C (0.04 g adsorbent, pH 3.0, 50 mg L^{-1} Cu(II)). After sampling, all solutions were filtered through 0.22 μm membranes immediately, and residual Cu(II) concentrations were measured by FAAS.

Adsorption capacity was calculated using the following formulas:[28]

$$q_t = \frac{(c_0 - c_t)}{m} V \quad (1)$$

$$q_t = \frac{(c_0 - c_e)}{m} V \quad (2)$$

where q_t (mg g^{-1}) and q_e (mg g^{-1}) denote adsorption capacities at time (t) and equilibrium, respectively; c_0, c_t, c_e (mg L^{-1}) represent initial, time (t), and equilibrium concentrations; V (L) is solution volume; m (g) is adsorbent mass.

2.5 Research on competitive adsorption

To evaluate the selectivity of E-CMBC for Cu(II), eight coexisting ions commonly present in industrial wastewater, namely Na^+, K^+, Ca^{2+}, and Mg^{2+}, were selected, and three types of concentration gradient experiments were set up: the initial concentration of Cu^{2+} was fixed at 50 mg L^{-1}, and the concentrations of single coexisting ions were set as 50 mg L^{-1} (molar ratio 1 : 1) and 500 mg L^{-1} (molar ratio 1 : 10), respectively. The experimental conditions were identical to those of the single Cu(II) adsorption system, *i.e.*, solution volume 100 mL, adsorbent dosage 0.4 g L^{-1}, initial pH 3.0, temperature 25 °C, shaking speed 150 r min^{-1}, and adsorption time 180 min. After preparing the mixed solution according to the designed concentrations and adjusting the pH, the adsorbent was added and the mixture was shaken. Upon reaching adsorption equilibrium, the solution was filtered through a 0.45 μm filter membrane. The equilibrium concentrations of Cu(II) and coexisting ions in the filtrate were determined by FAAS. Meanwhile, a blank control group and a single Cu(II) adsorption control group were established. The adsorption capacity was calculated using the previously described formula.

Distribution coefficient (K_d):

$$K_d = \frac{q_e}{c_e} \quad (3)$$

where q_e is the equilibrium adsorption capacity and c_e is the equilibrium concentration.

Selectivity coefficient (K):

$$K = \frac{K_d(\mathrm{Cu(II)})}{K_d(\text{coexisting ions})} \quad (4)$$

© 2026 The Author(s). Published by the Royal Society of Chemistry

Open Access Article. Published on 14 January 2026. Downloaded on 4/6/2026 1:23:54 AM. This article is licensed under a Creative Commons Attribution-NonCommercial 3.0 Unported Licence.

where K_d (Cu(II)) is the distribution coefficient of Cu(II) (L g^{-1}), K_d (coexisting ions) is the distribution coefficient of a single coexisting ion (L g^{-1}).

2.6 Regeneration study

To evaluate the reusability of E-CMBC, consecutive adsorption–desorption cycles were performed. After adsorption equilibrium, Cu(II)-loaded E-CMBC was separated, rinsed with deionized water, and then desorbed in 0.1 mol L^{-1} Na_2EDTA solution with overnight stirring.[29] The desorbed material was filtered, thoroughly washed with deionized water, and oven-dried. The regenerated E-CMBC was used for two more adsorption–desorption cycles under the same conditions.

3 Results and discussion

3.1 Characterization analysis

The surface morphologies of BC (unmodified biochar), MBC, CMBC, and E-CMBC are shown in Fig. 1. As seen in Fig. 1a, BC has a rough, porous structure. After modification with $FeSO_4$, MBC (Fig. 1b) shows many spherical Fe_3O_4 nanoparticles on its surface, confirming successful magnetic functionalization. The surface of CMBC (Fig. 1c) is covered with a dense polymer film, indicating that chitosan is grafted onto the surface of MBC through cross-linking reaction, forming a functionalized layer containing amino groups, which provides active sites for subsequent EDTA grafting.[30] Compared with the dense polymer membrane surface of CMBC, the surface roughness of E-CMBC increases significantly and forms raised nanostructures (Fig. 1d). This is due to the surface reconstruction caused by the increased steric hindrance of the molecular chains after EDTA is covalently grafted onto the chitosan molecular chains through amide bonds. This structure can increase the exposure and accessibility of adsorption sites, providing a structural basis for the rapid adsorption of Cu(II).

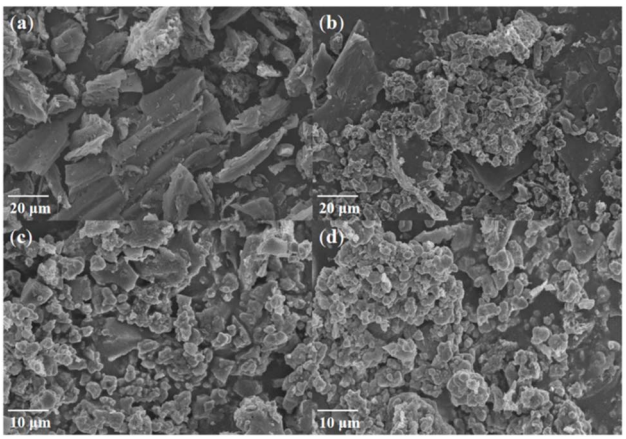

Fig. 1 Scanning electron microscopy images of (a) BC, (b) MBC, (c) CMBC and (d) E-CMBC.

Table 1 summarizes the surface area, pore volume, and average pore diameter of BC, MBC, CMBC, and E-CMBC. BC had the highest surface area (298.41 m^2 g^{-1}), which decreased to 143.74 m^2 g^{-1} after magnetization—likely due to partial pore blockage by Fe_3O_4 nanoparticles. Subsequent chitosan coating and EDTA modification further reduced the surface area, with a similar trend observed for pore volume. In contrast, MBC, CMBC, and E-CMBC had larger average pore diameters than BC, probably because smaller pores were preferentially blocked by magnetic particles and chitosan.[31]

Fourier-transform infrared (FT-IR) spectra (Fig. 2a) show surface chemical modifications. The characteristic peak at 571 cm^{-1} corresponds to Fe–O vibration, confirming the formation of Fe_3O_4.[32] The broad band near 3416 cm^{-1} comes from overlapping O–H and N–H stretching vibrations.[33] Peaks at 2850 cm^{-1} and 1067 cm^{-1} are attributed to aliphatic C–H stretching and C–O/C–C vibrations, respectively.[34] The significant enhancement of the COO^- symmetric stretching vibration peak at 1407 cm^{-1} (a characteristic functional group of EDTA) and the C–N stretching vibration peak at 1635 cm^{-1} (a characteristic functional group of chitosan) directly confirms that EDTA has been introduced onto the material surface through chemical grafting rather than physical mixing.[35] Distinct wavenumber changes post-Cu(II) adsorption indicate interactions between functional groups and Cu(II). For instance, the 3416 cm^{-1} peak (–NH_2/–OH stretching) broadens in CMBC-Cu (chitosan-modified) *vs.* MBC-Cu, and further in E-CMBC-Cu, confirming chitosan –NH_2 coordinates with Cu(II). Notably, the 1407 cm^{-1} peak (–COO^- bending of EDTA) emerges exclusively in E-CMBC-Cu, with slight intensity attenuation post-adsorption, indicating EDTA –COOH acts as a key chelating site.[36] These functional group changes (position/intensity) arise from Cu(II) interaction. The main adsorption mechanism involves complex formation between Cu(II) and N/O-containing groups (–NH_2 from chitosan, –COOH from EDTA).

XRD patterns (Fig. 2b) show characteristic diffraction peaks of Fe_3O_4 for MBC, CMBC, and E-CMBC at $2\theta = 30.1°$ (022), 35.4° (113), 43.1° (004), 56.9° (115), and 62.5° (044)—all matching the standard spinel structure of Fe_3O_4 (JCPDS no. 19-0629).[37,38] Notably, the intensity of these magnetic characteristic

Table 1 Textural properties and maximum Cu(II) adsorption capacities of BC, MBC, CMBC, and E-CMBC

Biochar	BET surface area (m^2 g^{-1})	Pore volume (cm^3 g^{-1})	Average pore size (nm)	Cu(II) adsorption capacity (mg g^{-1})
BC	298.41	0.06	5.58	33.92
MBC	143.74	0.033	6.98	42.78
CMBC	122.587	0.012	7.10	64.93
E-CMBC	114.303	0.016	6.22	130.8

Open Access Article. Published on 14 January 2026. Downloaded on 4/6/2026 1:23:54 AM.
This article is licensed under a Creative Commons Attribution-NonCommercial 3.0 Unported Licence.

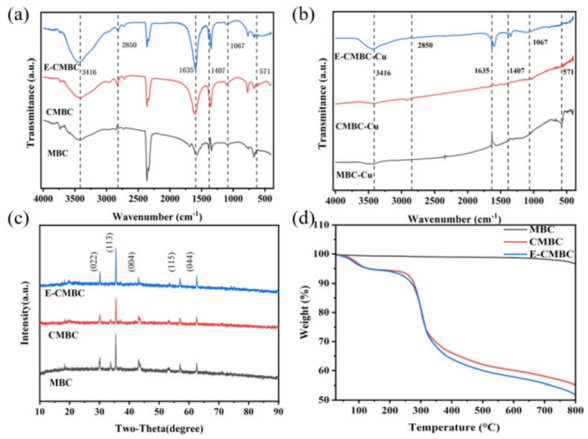

Fig. 2 (a and b) FTIR spectra of MBC, CMBC, and E-CMBC before and after Cu(II) ions adsorption, (c) XRD analysis for MBC, CMBC, and E-CMBC, (d) TGA curves of MBC, CMBC, and E-CMBC.

diffraction peaks does not weaken with subsequent chitosan coating and EDTA grafting. This confirms that Fe_3O_4 nanoparticles are stably anchored to the biochar framework through Fe–O–C bonds rather than physical adsorption. Such structural stability ensures the materials retain superparamagnetism both before and after Cu(II) adsorption, enabling rapid magnetic separation within seconds under an external magnetic field.

Thermogravimetric analysis (Fig. 2d) was conducted to evaluate the thermal stability of MBC, CMBC, and E-CMBC, while quantifying the grafting amount of modifiers and elucidating the modification-related thermal mechanism. In the low-temperature range (30–150 °C), all samples exhibited slight weight loss (5.1–6.7%), which was attributed to the removal of adsorbed surface water; notably, E-CMBC showed a marginally higher weight loss (6.7%) than CMBC (5.1%), a phenomenon ascribed to the hydrophilic –COOH groups introduced by EDTA, hinting at the successful incorporation of EDTA's characteristic functional groups onto the material surface. Moving to the moderate-temperature interval (150–450 °C)—the core region reflecting modification effects—pristine MBC showed negligible weight loss (<3%) as it lacked organic modifiers prone to thermal degradation, while CMBC exhibited 18.2% weight loss corresponding to the thermal fracture of chitosan's amino polysaccharide main chain (a signature of covalently grafted chitosan). For E-CMBC, this interval saw 23.1% weight loss; the 4.9% increment relative to CMBC aligned with the thermal decomposition of EDTA (300–450 °C, involving amide bond and carboxyl group fracture), directly quantifying EDTA's grafting amount (4.9%) and confirming EDTA was covalently grafted (physical mixing of EDTA would cause irregular low-temperature weight loss, which was not observed here). Finally, in the high-temperature range (450–800 °C), all samples underwent gradual weight loss (8–12%) due to the pyrolysis of the walnut shell biochar skeleton, and the residual mass (≈50–55% at 800 °C) mainly consisted of Fe_3O_4 magnetic particles and biochar ash, indicating that the bifunctional modification process did not destroy the basic structure of the magnetic biochar substrate.

3.2 Study on adsorption performance

3.2.1 Effect of initial pH. Solution pH significantly affects the surface charge of the adsorbent and the speciation of Cu(II), thus influencing adsorption. As shown in Fig. 3a, E-CMBC's adsorption capacity increased from 66.80 mg g^{-1} (pH 1.0) to 101.94 mg g^{-1} (pH 5.0), outperforming MBC and CMBC. When pH < 3, the high concentration of H^+ in the solution will cause protonation of the core adsorption sites (EDTA-COOH, chitosan-NH_2) on the surface of E-CMBC, making the surface of the adsorbent positively charged and generating electrostatic repulsion with Cu(II); meanwhile, H^+ will compete with Cu(II) for adsorption sites, resulting in a significant decrease in adsorption capacity.[39] The optimal performance at pH 5.0 is due to synergistic chelation by fully deprotonated when pH > 5, the increase in OH^- concentration in the solution will promote the hydrolysis of Cu(II) to form $Cu(OH)_2$ precipitate, and the concentration of free Cu(II) that can be adsorbed will decrease. At the same time, excessive OH^- will compete with Cu(II) for EDTA chelating sites, and the chitosan molecular chains are prone to cross-linking and agglomeration to encapsulate the adsorption sites, resulting in a decrease in adsorption efficiency.[40] The isoelectric point (pHPZC) of E-CMBC was determined to be approximately 2.3 by the zeta potential method (Fig. 3b). When pH > 2.3, the surface of the adsorbent becomes negatively charged, which is conducive to electrostatic attraction with positively charged Cu(II). When the pH is less than 2.3, the surface is positively charged and will generate electrostatic repulsion with Cu(II). The above-mentioned pH influence law is highly consistent with the characteristics of pHPZC. The effective adsorption range of pH 3 to 5 is precisely above pHPZC. At this time, the surface of the adsorbent carries a moderate negative charge, which not only avoids the protonation competition under strong acids but also does not reach the critical pH for Cu(II) hydrolysis, providing favorable conditions for efficient adsorption.

3.2.2 Effect of adsorbent dosage. Adsorbent dosage was inversely related to Cu(II) adsorption capacity (Fig. 3c). For E-CMBC, increasing the dosage from 0.02 g to 0.1 g decreased the capacity from 150.7 mg g^{-1} to 48.05 mg g^{-1}, while increasing the removal efficiency from 60.28% to 96.10%. An optimal dosage of 0.04 g (0.4 g L^{-1}) achieved a balance: 117.8 mg g^{-1} capacity with 94.23% removal—2–3 times more efficient than CMBC and MBC. Beyond 0.06 g, removal efficiency plateaued despite a 59.2% drop in capacity, indicating limited additional benefits. This dosage maximizes the synergy

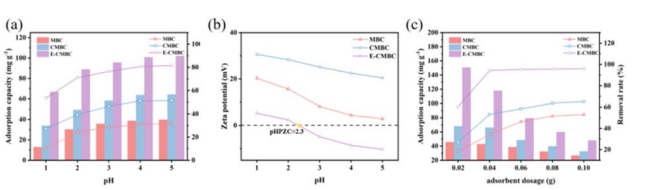

Fig. 3 Effects of initial solution pH (a), zeta potential under varying pH (b), and adsorbent dosage (c) on Cu(II) adsorption by MBC, CMBC, and E-CMBC.

© 2026 The Author(s). Published by the Royal Society of Chemistry

Open Access Article. Published on 14 January 2026. Downloaded on 4/6/2026 1:23:54 AM.
This article is licensed under a Creative Commons Attribution-NonCommercial 3.0 Unported Licence.

of bifunctional groups: EDTA chelation sites remain accessible, and chitosan networks facilitate mass transfer. In comparison, CMBC and MBC required 0.1 g to reach only 65.10% and 53.10% removal, respectively. Thus, 0.4 g L^{-1} was set as the optimal dosage.

3.3 Adsorption mechanism

3.3.1 Contact time and adsorption kinetics. Fig. 4 shows the effect of contact time on Cu(II) adsorption by the three materials. All adsorbents had increasing adsorption capacity over time, but with clear differences: E-CMBC reached 52.4% of its equilibrium capacity within 15 minutes and approached equilibrium at 120 minutes. In contrast, CMBC and MBC had much slower kinetics, showing that bifunctional modification accelerated adsorption by 2.7–3.9 times. To elucidate adsorption mechanisms, kinetic data were analyzed using pseudo-first-order (eqn (5)) and pseudo-second-order (eqn (7)) models. q_t values calculated using eqn (1) were fitted to the kinetic models by linear regression. This comparative modeling approach identified dominant mechanisms through regression coefficients (R^2).

Pseudo-first-order kinetic model formula:[41]

$$q_t = q_e(1 - e^{K_1 t}) \tag{5}$$

$$\ln(q_e - q_t) = \ln q_e - K_1 t \tag{6}$$

Pseudo-second-order model formula:[42]

$$q_t = \frac{K_2 q_e^{\,2} t}{1 + K_2 q_e t} \tag{7}$$

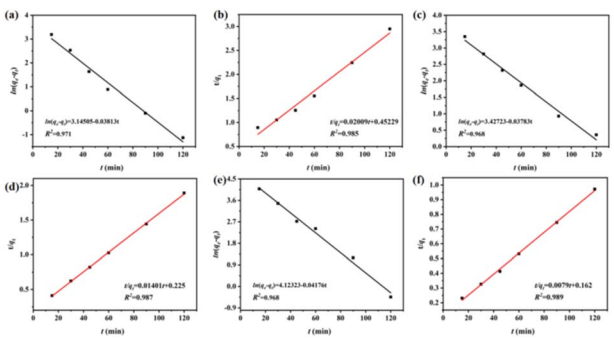

Fig. 4 Linearization of kinetic models: (a and b) pseudo-first-order and pseudo-second-order kinetics for MBC; (c and d) corresponding analysis for CMBC; and (e and f) corresponding analysis for E-CMBC.

$$\frac{t}{q_t} = \frac{1}{K_2 q_e^{\,2}} + \frac{t}{q_e} \tag{8}$$

where q_t represents the adsorbed amount at the moment of t, mg g^{-1}. q_e represents the saturated adsorbed amount at the time of equilibrium, mg g^{-1}. K_1 and K_2 are pseudo-first-order and pseudo-second-order kinetic rate constants in min^{-1} and g mg^{-1} min^{-1}, respectively.

Kinetic data were analyzed using the pseudo-first-order and pseudo-second-order models. The pseudo-second-order model had higher correlation coefficients ($R^2 > 0.98$) than the pseudo-first-order model for all adsorbents, indicating that chemical adsorption was dominant in the adsorption process of E-CMBC. Although MBC had a slightly higher pseudo-second-order rate constant than modified materials, its lowest equilibrium adsorption capacity (40.7 mg g^{-1}) reflected limited physical-chemical hybrid adsorption. In contrast, sequential modification of MBC with chitosan and EDTA increased the equilibrium adsorption capacity of E-CMBC to 124.16 mg g^{-1}—owing to the introduction of oxygen- and nitrogen-containing functional groups that enhanced the binding affinity of the material for Cu(II) (Table 2).

3.3.2 Adsorption isotherms. Adsorption isotherms describe equilibrium relationships between adsorbates and adsorbents. The Langmuir and Freundlich models are widely used for this purpose. The Langmuir model assumes monolayer coverage on homogeneous surfaces with finite active sites and no intermolecular interactions. In contrast, the Freundlich model characterizes multilayer adsorption on heterogeneous surfaces, demonstrating broader applicability across concentration gradients. Both models were fitted to experimental data to describe Cu(II) adsorption characteristics on E-CMBC. Their mathematical expressions are:

Langmuir equation:[43]

$$q_e = \frac{q_m K_L c_e}{1 + K_L c_e} \tag{9}$$

$$\frac{c_e}{q_e} = \frac{1}{q_m K_L} + \frac{c_e}{q_m} \tag{10}$$

Freundlich equation:[44]

$$q_e = K_F c_e^{\,1/n} \tag{11}$$

$$\ln q_e = \ln K_F + \frac{1}{n} \ln c_e \tag{12}$$

where q_e is the equilibrium adsorption amount, mg g^{-1}. c_e is the concentration of the solution when the reaction reaches

Table 2 Kinetic model parameters for adsorption of Cu(II) by MBC, CMBC and E-CMBC

		Pseudo-first-order kinetics			Pseudo-second-order kinetics		
Biochar	$Q_{e,exp}$ (mg g^{-1})	Q_e (mg g^{-1})	K_1 (min^{-1})	R^2	Q_e (mg g^{-1})	K_2 (g mg^{-1} min^{-1})	R^2
MBC	41.13	41.9	0.0381	0.971	42.6	0.0032	0.985
CMBC	64.93	66.5	0.0378	0.968	68.2	0.0023	0.987
E-CMBC	124.16	126.2	0.0409	0.968	126.6	0.0026	0.989

Open Access Article. Published on 14 January 2026. Downloaded on 4/6/2026 1:23:54 AM.
This article is licensed under a Creative Commons Attribution-NonCommercial 3.0 Unported Licence.

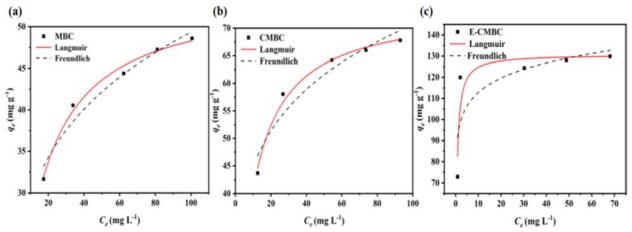

Fig. 5 Regression analysis of isotherm models: (a) fitting of Langmuir and Freundlich models for MBC, and comparative models for (b) CMBC and (c) E-CMBC.

Table 3 Adsorption equilibrium constants from Langmuir and Freundlich isotherms for Cu(II) adsorption by MBC, CMBC, and E-CMBC

	Langmuir model			Freundich model		
Biochar	Q_m (mg g^{-1})	K_L	R^2	n	K_F	R^2
MBC	49.106	0.08285	0.989	2.4	17.368	0.950
CMBC	71.007	0.12078	0.988	2.1	28.391	0.898
E-CMBC	130.828	2.05214	0.896	2.53	92.879	0.643

equilibrium, mg L^{-1}. q_m is the maximum adsorption amount, mg g^{-1}. K_L and K_F are Langmuir and Freundlich's adsorption affinity constants L mg^{-1}, respectively, and n denotes the adsorption strength factor.

As shown in Fig. 5 and Table 3, the maximum Langmuir adsorption capacity (130.828 mg g^{-1}) of E-CMBC was significantly higher than that of CMBC (71.007 mg g^{-1}) and MBC (49.106 mg g^{-1}). Its steep low-concentration profile and high Langmuir constant (K_L = 2.05214) indicated strong chemical adsorption at EDTA-chitosan bifunctional sites. Although the Langmuir R^2 (0.896) of E-CMBC is lower than that of the unmodified biochar, it remains higher than the Freundlich R^2 (0.839). This indicates that the adsorption process is dominated by monolayer adsorption, with minor characteristics of multilayer or non-uniform adsorption. The modification of E-CMBC constructs a bifunctional layer of "EDTA chelating site + chitosan-NH_2 coordination site". Both types of sites are specific metal binding sites and are uniformly distributed through directional crosslinking. This is the structural basis for its compliance with the Langmuir model (single molecular layer, uniform site). The Langmuir R^2 is lower than that of the unmodified material, mainly due to the contribution of a small number of non-specific adsorption sites (such as residual hydroxyl groups) on the surface of the adsorbent after the modification of the bifunctional layer, as well as the slight steric hindrance between the EDTA and chitosan molecular chains, which leads to differences in the accessibility of some adsorption sites and further introduces a small amount of non-uniform adsorption behavior. Make the Freundlich model also present a certain degree of fit. CMBC and MBC had gradual isotherm profiles with high fits, consistent with physical adsorption. This shows that bifunctional modification changed the mechanism from passive physical adsorption to chemical chelation, increasing capacity by 84.2%.

3.3.3 Adsorption thermodynamics. Thermodynamic analysis explains temperature-dependent adsorption behavior. Key parameters—Gibbs free energy change (ΔG), enthalpy change (ΔH), and entropy change (ΔS)—were calculated using the following equations:

$$K_d = \frac{q_e}{c_e} \quad (13)$$

$$\ln K_d = \frac{\Delta S}{R} - \frac{\Delta H}{RT} \quad (14)$$

$$\Delta G = \Delta H - T \times \Delta S \quad (15)$$

where q_e (mg g^{-1}) is equilibrium adsorption capacity, c_e (mg L^{-1}) is equilibrium concentration, K_d is the distribution coefficient (q_e c_e), R (8.314 J mol^{-1} K) is the gas constant, and T (K) is absolute temperature.

As shown in Table 4, increasingly negative ΔG values with rising temperature indicated that the adsorption process became more spontaneous at higher temperatures—a characteristic of chemical adsorption. ΔH is 20.94 kJ mol^{-1} (>0), confirming that adsorption is an endothermic reaction, and an increase in temperature is conducive to the adsorption process. ΔS is 106.5 J mol^{-1} K^{-1} (>0), indicating that chemical chelation dominates the adsorption process, accompanied by ion exchange (for example, between Cu(II) and H^+ on a protonated functional group). The migration and redistribution of ions at the solid–liquid interface increase the fluidity of particles in the system and promote the increase of entropy.

3.4 Study on competitive adsorption and selectivity

Actual wastewater usually contains multiple coexisting cations, which compete with target heavy metal ions for adsorption sites. To evaluate the potential of E-CMBC in practical applications, this study investigated the effects of common background electrolytes (Na^+, K^+, Ca^{2+}, Mg^{2+}) on Cu(II) adsorption. The results are shown in Fig. 6 and Table 5. Fig. 6 visually presents the influence trend of different interfering ions and concentration ratios on the removal efficiency of Cu(II), while Table 5 quantifies the differences in adsorption affinity and selectivity. Both jointly confirm that the selectivity of E-CMBC shows a significant "valence state dependence" characteristic: it has extremely strong selectivity for monovalent Na^+ and K^+. Even under 10 times high concentration interference, the selectivity coefficient K still exceeds 20, and the K_d (Cu(II)) (47.12–49.58 L g^{-1}) is more than 20 times that of the interfering ions. The selectivity for divalent Ca^{2+} and Mg^{2+} is relatively mild.

Table 4 Thermodynamic parameters for the adsorption of Cu(II) by E-CMBC

T (K)	K_d (L g^{-1})	ΔG (kJ mol^{-1})	ΔH (kJ mol^{-1})	ΔS (J mol^{-1} K)
298	76.62	−11.2	20.94	106.5
308	133.37	−13.1		
318	302.37	−14.9		

© 2026 The Author(s). Published by the Royal Society of Chemistry

Open Access Article. Published on 14 January 2026. Downloaded on 4/6/2026 1:23:54 AM.
This article is licensed under a Creative Commons Attribution-NonCommercial 3.0 Unported Licence.

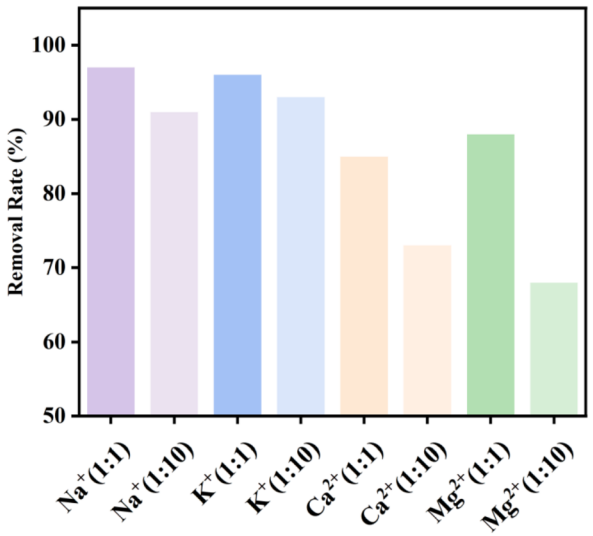

Fig. 6 Effect of competitive ions on the efficiency of Cu(II) removal by E-CMBC.

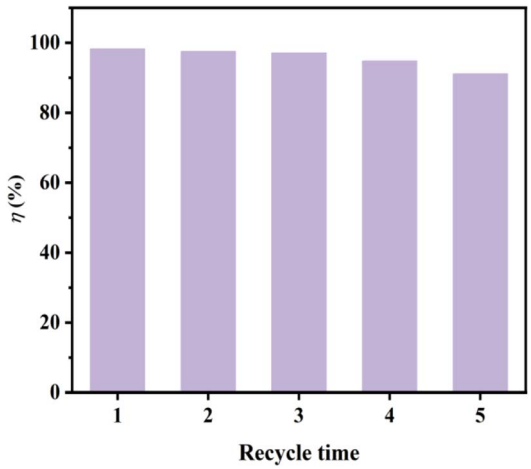

Fig. 7 Desorption and regeneration effects of E-CMBC.

Under 10 times the interference, the K value drops to 1.86–2.33, but K_d (Cu(II)) (13.96–16.85 L g^{-1}) is still higher than that of the interfering ions. This difference is essentially determined by the specific mechanism of action of E-CMBC.

The high selectivity of E-CMBC for Cu(II) stems from the synergistic effect of EDTA chelation specificity, chitosan coordination preference and bifunctional layer spatial screening, which is also the core support for its anti-interference ability. The six-tooth chelating structure of EDTA is highly compatible with the configuration of Cu(II) ions, which can form a stable chelating ring with the least tension. This structural specificity makes its binding priority for Cu(II) much higher than that of Ca^{2+} and Mg^{2+}, which can only form weak complexes, and it is even more unable to form effective complexes with Na^+ and K^+. Meanwhile, the $-NH_2$ on the chitosan molecular chain has a specific spatial configuration, and its ionic radius compatibility with Cu(II) is better than that of Na^+ and K^+. Moreover, it has coordination repulsion for Ca^{2+} and Mg^{2+} with lower charge densities, further strengthening the targeted binding to Cu(II). The bifunctional layer formed by the cross-linking of EDTA and chitosan also builds a "Cu(II) affinity" microenvironment. The $-NH_2$ of chitosan first enriches Cu(II) in the solution through electrostatic interaction to lower the diffusion energy barrier, and then guides Cu(II) to preferentially bind to the chelation sites of the inner EDTA, forming a "enrichment-chelation" relay effect. Ultimately, the selective difference for Cu(II) is magnified. It is precisely this synergistic mechanism that enables E-CMBC to maintain its adsorption advantage for Cu(II) even under high-concentration interference, providing performance guarantee for the actual treatment of copper-containing wastewater.

3.5 Regeneration and reusability study

The reusability of an adsorbent is a crucial practical characteristic. We subsequently tested E-CMBC through consecutive adsorption–desorption cycles for Cu(II) removal. As shown in Fig. 7, after five cycles, E-CMBC maintained a high Cu(II) removal efficiency of 91.13%. The EDTA modification appears to have stabilized the adsorbent, enhancing its resilience in acidic conditions. These results demonstrate the excellent reusability potential of E-CMBC (Table 6).

3.6 Mechanism

Based on the comprehensive analysis of the aforementioned characterization results and adsorption performance studies, the efficient adsorption of Cu(II) by the E-CMBC constructed in this study is not dominated by a single mechanism, but rather

Table 5 The influence of different coexisting ions on the K_d and selectivity coefficient of Cu(II) adsorption by E-CMBC

Coexisting ion types	Coexisting ions	Concentration ratio (Cu: coexisting ion)	K_d (Cu(II)) (L g^{-1})	K_d (coexisting ion) (L g^{-1})	Selectivity coefficient (K)
Alkali metal ions	Na^+	1 1	80.83	2.31	35.0
		1 10	47.12	2.15	22.0
	K^+	1 1	77.45	2.54	30.5
		1 10	49.58	2.42	20.5
Alkaline earth metal ions	Ca^{2+}	1 1	34.23	6.87	4.98
		1 10	16.85	7.23	2.33
	Mg^{2+}	1 1	38.61	7.12	5.42
		1 10	13.96	7.51	1.86

© 2026 The Author(s). Published by the Royal Society of Chemistry

Open Access Article. Published on 14 January 2026. Downloaded on 4/6/2026 1:23:54 AM. This article is licensed under a Creative Commons Attribution-NonCommercial 3.0 Unported Licence.

Table 6 Comparison of the adsorption performance of chitosan or EDTA modified adsorbents for Cu(II)

Type of adsorbent	Modification method	Cu(II) adsorption capacity (mg g^{-1})	Key adsorption conditions	References
CMBC	Chitosan modification	68.2	Adsorbent dosage 0.04 g, solution volume 50 mL, initial concentration 50 mg L^{-1}, adsorption time 180 minutes, 25 °C	Present study
EDTA-chitosan modified sewage sludge	One-step cross-linking method (EDTA + chitosan modified sewage sludge)	42.4	pH 3.0, adsorbent dosage 0.02 g, adsorption time 270 minutes, 25 °C	45
N,*O*-carboxymethyl chitosan (*N*,*O*-CMC)	Carboxymethylation (α-ketoglutarate modification)	30.2	pH 5.0, adsorbent dosage 0.05 g, solution volume 50 mL, initial concentration 25–100 ppm, adsorption time 360 minutes, 25 °C	46
E-CMBC	Construction of a bifunctional layer with EDTA chelation and chitosan-NH_2 coordination	130.8	Adsorbent dosage 0.04 g, solution volume 50 mL, initial concentration 50 mg L^{-1}, adsorption time 180 minutes, 25 °C	Present study
EDTA-BIOC hydrogel	Biochar is activated by nitric acid acidification; preparation of BIOC by acylation reaction grafting ethylenediamine (EDA); graft EDTA to introduce chelating sites; with acrylamide (AM), acrylic acid (AA) free radical polymerization, HF etching SiO_2 to increase porosity	93.9	pH = 6, adsorbent dosage 0.03 g, adsorption time 80 minutes, 45 °C	47

the result of the combined multiple mechanisms, with dual-functional coordination as the core. Its adsorption mechanism can be conceptually summarized in Fig. 8. Surface complexation/chelation is the core mechanism among them. The EDTA molecules and chitosan chains grafted on the material surface provide abundant nitrogen-containing and oxygen-containing functional groups (such as $-NH_2$, $-COOH/-COO^-$), which can act as electron donors to form stable inner-sphere complexes or chelates with Cu(II) ions. This is confirmed by the extremely high Langmuir adsorption capacity (130.8 mg g^{-1}), fitting constant (K_L), and the compliance with the pseudo-second-order kinetic model. Meanwhile, ion exchange plays an important role: under acidic or near-neutral conditions, H^+ on the protonated carboxyl groups (–COOH) or hydroxyl groups (–OH) in EDTA and chitosan molecules, as well as other exchangeable cations that may exist on the material surface (such as Na^+ introduced during the preparation process), can undergo an exchange reaction with Cu^{2+} in the solution, thereby immobilizing Cu(II) on the material surface. The electrostatic attraction mechanism also plays a crucial role. Solution pH experiments and zeta potential analysis show that at relatively high pH values, the material surface is deprotonated and carries a negative charge (in the form of $-COO^-$), which interacts with Cu(II) through coulombic attraction to promote the adsorption process. In addition, although the specific surface area of the material decreases after modification, its inherent porous structure can still provide attachment sites and diffusion channels for Cu(II) ions through pore filling and physical adsorption. Through its unique structure, E-CMBC achieves a multi-mechanism adsorption process dominated by dual-functional coordination, with ion exchange, electrostatic attraction, and physical adsorption serving as synergistic assistants.

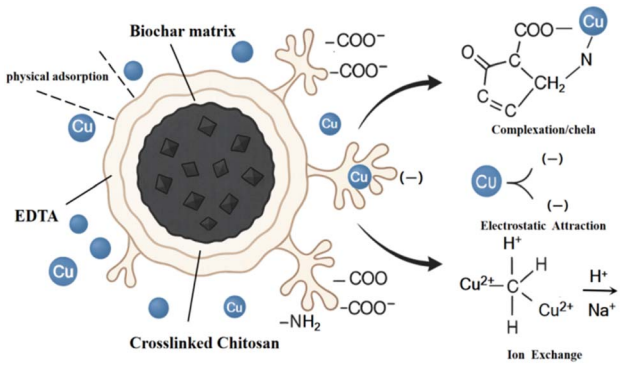

Fig. 8 Proposed adsorption mechanism of Cu(II) by E-CMBC.

4 Conclusion

This study constructed a chitosan-EDTA bifunctionalized magnetic walnut shell biochar (E-CMBC), which significantly enhanced the adsorption performance for Cu(II). Under

© 2026 The Author(s). Published by the Royal Society of Chemistry

Open Access Article. Published on 14 January 2026. Downloaded on 4/6/2026 1:23:54 AM. This article is licensed under a Creative Commons Attribution-NonCommercial 3.0 Unported Licence.

optimized conditions (pH = 5.0, 40 °C, 0.4 g L^{-1}), the maximum adsorption capacity reached 130.8 mg g^{-1}, representing a 2.66-fold improvement compared to the unmodified material, with 52.4% of the equilibrium capacity achieved within 15 minutes. The mechanism was confirmed to be dominated by dual-functional coordination between carboxyl groups of EDTA and amino groups of chitosan, leading to chemisorption, while the spontaneous endothermic process was primarily driven by entropy increase. The material exhibited superparamagnetism and excellent regenerability, with strong applicability in the pH range of 3–5 and at room temperature. Studies on competitive adsorption showed that E-CMBC exhibits high selectivity for Cu(II): the coexisting Na^+ and K^+ have almost no effect, while the influence of Ca^{2+} and Mg^{2+} is limited. This demonstrates its promising application prospect in practical wastewater treatment. This strategy provides an efficient solution for heavy metal pollution control and high-value utilization of agricultural and forestry waste, though future work will focus on enhancing its adaptability in highly acidic environments.

Author contributions

Xuejian Zhou: writing– original draft, methodology, data curation, conceptualization. Yufei Yang: investigation, data curation. Ruiqi Yang: investigation, formal analysis, conceptualization. Lei Shi: methodology, conceptualization. Ling Zhou, Xifeng Lv: review & editing, validation, methodology, funding acquisition. All authors have read and agreed to the published version of the manuscript.

Conflicts of interest

The authors declare no conflicts of interest.

Data availability

The original contributions presented in this study are included in the article. Further inquiries can be directed to the corresponding authors.

Acknowledgements

This work is financially supported by Corps Major Science and Technology Program (2024AA008); Provincial Science and Technology Key Projects (2025AB005); Science and Technology Program of XPCC (2025BC010) and Tarim University Presidential Fund (ZNLH202601).

References

1 S. Huang, Z. Lu, X. Zhao, W. Tan, H. Wang, D. Liu and W. Xing, *Agriculture*, 2024, **14**, 914.
2 J. He, Y. Yang, G. Christakos, Y. Liu and X. Yang, *Geoderma*, 2019, **337**, 359–367.
3 H. Hu, Q. Jin and P. Kavan, *Sustainability*, 2014, **6**, 5820–5838.
4 A. Aklil, M. Mouflih and S. Sebti, *J. Hazard. Mater.*, 2004, **112**, 183–190.
5 E. Vunain, A. K. Mishra and B. B. Mamba, *Int. J. Biol. Macromol.*, 2016, **86**, 570–586.
6 N. K. Srivastava and C. B. Majumder, *J. Hazard. Mater.*, 2008, **151**, 1–8.
7 X. Gong, D. Huang, Y. Liu, G. Zeng, R. Wang, J. Wei, C. Huang, P. Xu, J. Wan and C. Zhang, *Bioresour. Technol.*, 2018, **253**, 64–71.
8 Y. Liu, R. Zhang, Z. Sun, Q. Shen, Y. Li, Y. Wang, S. Xia, J. Zhao and X. Wang, *Environ. Pollut.*, 2021, **272**, 115978.
9 X. Ren, C. M. Pan, Z. M. Pan, S. S. Zhao, C. Wu, W. Chen, M. C. Liu, X. Y. Han, H. Y. Kuang and M. Qu, *Medicine*, 2022, **101**, e31133.
10 I. Scheiber, R. Dringen and J. F. B. Mercer, in *Interrelations between Essential Metal Ions and Human Diseases*, ed. A. Sigel, H. Sigel and R. K. O. Sigel, Springer Netherlands, Dordrecht, 2013, pp. 359–387, DOI: 10.1007/978-94-007-7500-8_11.
11 R. Foroutan, S. J. Peighambardoust, R. Mohammadi, S. H. Peighambardoust and B. Ramavandi, *Chemosphere*, 2022, **296**, 133978.
12 S. J. Peighambardoust, A. Hamdi, P. Mohammadzadeh Pakdel and N. S. Peighambardoust, *Inorg. Chem. Commun.*, 2025, **173**, 113797.
13 W. Liao, Q. Zhao, H. Chen, C. Liao, Y. Wang and X. Wang, *Energy Convers. Manage.*, 2019, **199**, 111965.
14 A. Bashir, L. A. Malik, S. Ahad, T. Manzoor, M. A. Bhat, G. Dar and A. H. Pandith, *Environ. Chem. Lett.*, 2019, **17**, 729–754.
15 J. P. Bezzina, L. R. Ruder, R. Dawson and M. D. Ogden, *Water Res.*, 2019, **158**, 257–267.
16 S. A. Rahmaninezhad, N. Mehrdadi and Z. Mahzari, *J. Aust. Ceram. Soc.*, 2021, **57**, 163–172.
17 M. Kobya, E. Demirbas, E. Senturk and M. Ince, *Bioresour. Technol.*, 2005, **96**, 1518–1521.
18 H.-M. Lee, B.-H. Lee, J.-H. Kim, K.-H. An, S.-J. Park and B.-J. Kim, *Carbon Lett.*, 2019, **29**, 649–654.
19 S. Edebali and E. Pehlivan, *Powder Technol.*, 2016, **301**, 520–525.
20 K. Adegoke, S. Akinnawo, T. Adebusuyi, O. Ajala, R. Adegoke, N. Maxakato and O. Bello, *Int. J. Environ. Sci. Technol.*, 2023, **20**, 11615–11644.
21 L. Ramrakhiani, S. Ghosh and S. Majumdar, *Appl. Biochem. Biotechnol.*, 2016, **180**, 41–78.
22 J. Yang, B. Hou, J. Wang, B. Tian, J. Bi, N. Wang, X. Li and X. Huang, *Nanomaterials*, 2019, **9**, 424.
23 M. Rinaudo, *Prog. Polym. Sci.*, 2006, **31**, 603–632.
24 F. H. Emamy, A. Bumajdad and J. P. Lukaszewicz, *Nanomaterials*, 2021, **11**, 1907.
25 M. E. Peralta, R. Nisticò, F. Franzoso, G. Magnacca, L. Fernandez, M. E. Parolo, E. G. León and L. Carlos, *Adsorption*, 2019, **25**, 1337–1347.
26 S. T. Zhuang, Q. Zhang and J. L. Wang, *J. Mol. Liq.*, 2021, **325**, 115197.
27 Y. Wang, F. H. Wang, L. Shu, P. Wu, Z. J. Li, J. F. Gao and H. H. Liu, *Water, Air, Soil Pollut.*, 2023, **234**, 131.

© 2026 The Author(s). Published by the Royal Society of Chemistry

Open Access Article. Published on 14 January 2026. Downloaded on 4/6/2026 1:23:54 AM.
This article is licensed under a Creative Commons Attribution-NonCommercial 3.0 Unported Licence.

28 L. Tan, Y. Nie, H. Chang, L. Zhu, K. Guo, X. Ran, N. Zhong, D. Zhong, Y. Xu and S.-H. Ho, *Bioresour. Technol.*, 2024, **394**, 130287.
29 B. Chen, H. Zhao, S. Chen, F. Long, B. Huang, B. Yang and X. Pan, *Chem. Eng. J.*, 2019, **356**, 69–80.
30 D. Hu, Z. Lian, H. Xian, R. Jiang, N. Wang, Y. Weng, X. Peng, S. Wang and X. K. Ouyang, *Int. J. Biol. Macromol.*, 2020, **154**, 1537–1547.
31 N. Yin, Y. Ai, Y. Xu, Y. Ouyang and P. Yang, *J. Radioanal. Nucl. Chem.*, 2020, **326**, 1307–1321.
32 J. H. Ning, D. E. Chen, Y. L. Liu, S. E. Huang, F. X. Wang, R. Wei, Q. C. Hu, J. Q. Wei and C. Sun, *J. Cent. South Univ.*, 2021, **28**, 3666–3680.
33 K. Oktor, N. Y. Yuzer, G. Hasirci and N. Hilmioglu, *Water, Air, Soil Pollut.*, 2023, **234**, 271.
34 Y. C. Dong, P. Wang, L. Gan, B. Li and H. J. Wen, *Cellulose*, 2019, **26**, 7383–7397.
35 J. H. Wang, D. Zhang, S. C. Liu and C. Y. Wang, *Sci. Total Environ.*, 2020, **720**, 137391.
36 R. Shahrokhi-Shahraki, C. Benally, M. G. El-Din and J. Park, *Chemosphere*, 2021, **264**, 128455.
37 Y. Jia, Y. Zhang, J. Fu, L. Yuan, Z. Li, C. Liu, D. Zhao and X. Wang, *Colloids Surf., A*, 2019, **567**, 278–287.
38 S. Ye, M. Cheng, G. Zeng, X. Tan, H. Wu, J. Liang, M. Shen, B. Song, J. Liu, H. Yang and Y. Zhang, *Water Res.*, 2020, **179**, 115876.
39 M. Hassan, Y. Liu, R. Naidu, S. J. Parikh, J. Du, F. Qi and I. R. Willett, *Sci. Total Environ.*, 2020, **744**, 140714.
40 Y. Jin, M. Zhang, Z. Jin, G. Wang, R. Li, X. Zhang, X. Liu, J. Qu and H. Wang, *Environ. Res.*, 2021, **196**, 110323.
41 E.-B. Son, K.-M. Poo, J.-S. Chang and K.-J. Chae, *Sci. Total Environ.*, 2018, **615**, 161–168.
42 E.-J. Lee and J.-W. Lee, *Bioresour. Technol.*, 2024, **407**, 131124.
43 D. H. Sun, X. D. Zhang, Y. D. Wu and X. Liu, *J. Hazard. Mater.*, 2010, **181**, 335–342.
44 R. Tang, C. Dai, C. Li, W. Liu, S. Gao and C. Wang, *J. Chem.*, 2017, **2017**, 8404965.
45 J.-H. Wang, S. Atif, Y. Chen and R. Guo, *Desalin. Water Treat.*, 2020, **190**, 167–178.
46 M. E.-S. Abdel-Raouf, R. K. Farag, A. A. Farag, M. Keshawy, A. Abdel-Aziz and A. Hasan, *Acs Omega*, 2023, **8**, 10086–10099.
47 J. Li, K. Li, J. Yan and T. Zhou, *New J. Chem.*, 2022, **46**, 14127–14139.

© 2026 The Author(s). Published by the Royal Society of Chemistry